Structure and Performance of Filter Media

H. P. GRACE

E. I. du Pont de Nemours & Co., Wilmington, Delaware

I. The Internal Structure of Filter Media

The internal structure of various types of filter media and the nature of fluid flow through them are examined. Methods of characterizing the internal pore structure of filter media are reviewed, and the permeability, bubble-pressure, and mercury-intrusion methods are applied to ten typical media, with resulting values of average and maximum pore radius and pore-size distribution being reported. These data on internal pore structure are related to the construction variables characteristic of the media examined, in particular the effect of yarn construction, yarn twist, fabric weave, and fabric finish on textile-type filter media.

The filter medium is an essential and very critical component of every filtration step and can make or break it from either an economic or a performance standpoint. Commercial filter media have been developed through the trial of hundreds of textile fabrics and other porous materials. Most of these were originally intended for other purposes, but through experience some five hundred or more have been found useful for filtering liquids. New filter media continue to evolve by this means. Few engineering criteria exist for the selection of existing filter media or for the design and construction of new media for efficient performance in the various types of filtration service. This lack of a quantitative basis for both the design and selection of filter media is largely responsible for the wide and continually changing variety of filter media in general use.

Experimental procedures for correlating physical characteristics, internal structure, and performance are needed before any major improvement in this situation can be expected. A means of quantitatively relating these factors should result eventually in the design of the best filter media for particular types of service. The immediate objectives of the work reported in Parts I and II of this paper were the development and application of techniques for evaluating pore structure and functional performance of filter media and the correlation of these factors with each other and with other measured properties of filter media.

STRUCTURE OF FILTER MEDIA

Filter media can be divided into three general classes: (1) a wide variety of woven textile fabrics, (2) random-packed beds of a fibrous material (including compacted or mechanically bound beds such as pressed felts, paper, and nonwoven fabrics), and (3) random-packed beds of rigid particles (including pressed and/or sintered compacts of such materials). Media composed of random-packed beds exhibit a highly random distribution of pore volume, show a great tortuosity of interconnecting pore structure, and are probably composed of interconnecting pores which contract and expand continually along any path through the medium. By contrast, woven filter media exhibit a highly oriented structure and are composed of distinctly different interyarn and interfiber pores, many of which are probably less tortuous than those through a packed bed.

General experience has indicated that to be a practical filter medium, a packed bed must be composed of particles or fibers appreciably larger, in at least one dimension, than the particles to be removed and that the particles or fibers in the packed bed must be of such a size and shape distribution that the packed bed is of a high porosity even when subjected to normal filtration pressure drop. Only meager information is available on the use of packed beds (other than sand beds for water clarification, which is a special case) as the medium for liquid filtration. Filter aids have been studied by Carman (*7*), Cummins (*9*), and Hoffing and Lockhardt (*21*), but principally as additives to increase filter-cake permeability; their use in precoat form as the filter medium itself and the physical properties of such precoat beds have not been considered. The relationship between particle removal from a passing gas stream and the structure of filter

beds of fibers has been considered theoretically by Langmuir (*27*) and Davies (*11*), whose work has been well summarized by Thomas (*43*). However, their work does not consider the effect of bed structure on the rate of plugging even for gas filtration and may not be generally applicable to liquid clarification because of differences in the basic mechanism of particle collection and retention. Thus the need for information on the structure and performance of packed beds as filter media for liquids appears second only to the need for similar information on woven filter media.

While woven filter media are more widely used for liquid filtration than are packed-bed media, the weavers and vendors have little knowledge of internal pore structure and the effect of construction variables (such as filament or staple denier, number of filaments, yarn packing structure and twist, plying of yarns, type of weave structure, and various finishing operations) on either the pore structure or the functional performance of the medium. Recently Schwarz (*38*) considered the effect of yarn structure on fabric properties. He points out that only a few of the various types of possible fiber-packing arrangements are sufficiently stable for good results, and he presents micrographs of sections of single and plied yarns which show the nature of interfiber voids with various yarn structures and yarn twists. He concludes that, in general, decreasing filament denier, increasing the number of filaments per yarn, and increasing yarn twist, all tend toward producing a smaller and more uniform interfiber void, although a design yielding a stable packing arrangement is an essential first requirement. More recently Hoffman (*22*) has considered the effect of fabric design and construction on the density, or porosity, of both the yarns and the over-all fabric. He predicts that a range of filament denier in the yarn structure will result in greater yarn porosity and larger interfiber voids because of a "wedging-apart" action. Hoffman also emphasizes the practical importance of the flattened or elliptical cross section of yarns when considered in the actual fabric and shows section views of various fabrics to illustrate this important point. This elliptical shape is characteristic of tight fabrics such as filter media and is further promoted by fabric-finishing procedures such as calendering. According to Hoffman, increasing yarn twist alone results in a thicker fabric, a lower porosity yarn, a more open weave, and a more nearly circular yarn within the fabric.

Backer (*3*) has shown the general effect of interyarn geometry (i.e., weave construction) on shape and area of pores at various cross sections through the fabric and has related these to the permeability characteristics of certain fabrics. Smith (*42*) in a recent discussion of filter-media properties and performance emphasizes the role of high yarn twist in reducing the volume of interfiber pores and the importance of filtering through interyarn instead of interfiber pores to prevent cloth plugging in cake filtrations. Silverman (*41*) has emphasized the importance of fiber diameter and total specific surface of the filter medium in removing small dust particles from dilute-gas suspensions. These factors, however, merely form a method of expressing effective pore radius in terms of fiber properties but fail to take into account yarn and weave construction, which also influences pore radius.

FLOW THROUGH FILTER MEDIA

Initial considerations require a knowledge of the flow and flow resistance with unused media before any understanding can be achieved of flow during the blocking period of actual filtration. For packed beds of fibers or solid particles, a large amount of information is available on correlation of flow resistance with bed properties, and this was reviewed recently as applied to filtration (*19*). For woven-filter media the picture is complicated by the highly oriented nature of the fiber packing. The idealized case of a monofilament weave, as represented by screens, has been treated by several workers (*20*, *32*, and *36*) and by a screen manufacturer (*1*). These treatments are all similar and are based on development of a correlation of discharge coefficient vs. Reynolds number and the fractional free area represented by interyarn pores.

Robertson (*36*) has attempted to extend this treatment to multifilament and staple yarn fabrics with only limited success. For plain weaves of rather open construction, correlation by this method was fairly satisfactory, but for more complex weaves and particularly for weaves of tightness approaching that of most woven filter media, the method failed badly. This probably results from the fact that as interyarn pores become smaller or more tortuous, an appreciable amount of fluid flows through the interfiber pores in parallel with the interyarn pores. Data on various filter media have shown that while values for air flow and liquid flow through monofilament media usually agreed, with multifilament and staple-yarn media the resistance to liquid flow is almost always considerably greater than would have been predicted from the air-flow resistance. In some cases this discrepancy results largely from swelling of the fibers in the liquid. In many cases with synthetic fibers, however, swelling is not a factor, and this discrepancy is believed to result from the division of flow between parallel interyarn and interfiber pores and from possible slip flow of air in the interfiber pores. Recent results of Cunningham et al. (*10*) have further confirmed this observed discrepancy and have suggested that wetting phenomena may also be involved.

No sound data are available on this division of flow with tightly woven media, and literature reports are conflicting. Robertson (*36*) reports that complete plugging of interfiber pores of such media decreased permeability only 10% and Smith (*42*) reports that complete plugging of interfiber pores reduced permeability 95 to 98% with similar low-twist fabrics. Probably the magnitude of the effect even with tightly woven fabrics is largely dependent on many factors involved in fabric construction. Backer (*3*) has considered the effect of many of these design factors on division of flow through interfiber and interyarn pores and over-all permeability. He concluded that more numerous interlacing of the yarn system (higher fabric count) reduces permeability by simultaneously reducing the size of both interyarn and interfiber pores, other factors remaining constant. On the other hand, Robertson (*36*) found that if all elements other than twist are held constant, the permeability increases as the twist is increased even though the interfiber pores decreased in size with increasing twist. An explanation of this may be that as the twist increases and interfiber pore size decreases, the interyarn pore size increases, and the division of flow shifts more to the interyarn pores.

Rainard (*35*), in correlating air-permeability data in textile fabrics, has taken a different approach from that of most other workers. On the basis of his data, he proposes an empirical equation of the form

$$(70.6)\ \frac{\Delta p_f}{q_f} = C_1 q_f + C_2 \qquad (1)$$

This is similar in form to equations proposed more recently by Durwez and Green (*15*) to describe flow through metal compacts and by Ergun (*17*) to describe flow through packed columns. Although Rainard's data were insufficient to define the exact nature of C_1 and C_2, he suggested on theoretical grounds that

$$C_1 = \frac{b\rho_f}{g_c \pi^2 r^4 N^2 A^2}\,(10)^{16} \qquad (2)$$

$$C_2 = \frac{8h\mu_f}{g_c \pi r^4 N A}\,(10)^{14} \qquad (3)$$

where b is a constant to account for the variation in velocity resulting from expansions and contractions along the length of the pores. Actually the empirically determined values of C_1 obtained by Rainard were probably also a function of the distribution of flow between interfiber and interyarn pores.

PORE-SIZE MEASUREMENT

The size distribution, shape, tortuosity, and volume of pores in a filter medium

are of prime importance to the retentiveness, flow resistance, and plugging rate in filtration service. Available information also indicates that a knowledge of these properties is an essential intermediate link between the performance properties of a medium and the construction of the medium. Initial work on this problem resulted in development and application of procedures for measuring average and maximum pore size of woven media. The values of average pore radius so obtained are calculated from liquid-permeability data for the viscous-flow range employing a modification of the Kozeny-Carman relationship. Thus for a circular pore of radius r, the hydraulic radius

$$m = r_p/2$$

and

$$r_p = \frac{2\epsilon}{(1-\epsilon)S_0}(10)^4 \qquad (4)$$

where S_0 can be calculated from the resistance coefficient of the medium by employing the Kozeny-Carman relationship in the form

$$S_0^2 = \frac{\epsilon^3}{(1-\epsilon)^2 K}\frac{(R_m')}{(L)}(1.075 \times 10^3) \qquad (5)$$

The resistance coefficient of the filter medium R_m' is calculated from liquid-permeability data in the viscous-flow range by use of the relationship

$$R_m' = (2.16 \times 10^5)\frac{A g_c \Delta p_w}{\mu_f q_f} \qquad (6)$$

The pore radius so obtained is probably an average falling between the radius of interfiber pores and that of interyarn pores, but on a comparative basis these values have proved very useful in selection of filter media. A similar method has been used recently by Schwertz (*39*) to determine average pore size and pore-population density of fritted-glass filter disks; however, gases were used instead of liquid and this necessitated use of a slip-flow correction of uncertain accuracy. Other methods of calculating an average pore radius from permeability data have been employed by many workers dealing with membranes (*16, 28, 29, 31*). This method assumes that pores are straight-through, parallel capillaries of length equal to the membrane thickness. With this assumption, Poiseuille's law can be transformed to yield a pore radius directly,

$$r_p = \frac{(8L)^{1/2}}{(\epsilon R_m')}(30.5 \times 10^4) \qquad (7)$$

Although this method has been applied to calculate pore sizes in sintered ceramic filters (*12*), such use is difficult to reconcile with the basic assumption of straight-through pores made in its derivation. Thus this method does not appear so applicable to either woven or packed-bed filter media as does the modified Kozeny-Carman relationship.

Measurement of size of maximum pore by the bubble-pressure method is not new and has been widely applied to membranes (*4* and *30*) and fine structure of porous ceramic bodies (*26* and *2*). More recently it has been applied to textile fabrics (*39*) in studies relating to their water repellency. The bubble method depends simply on equating forces at the entrance to a liquid-filled capillary. Thus if a circular pore cross section is assumed, the radius of maximum pore is calculated from

$$r_m = (0.1448)\frac{2\sigma \cos\theta}{\Delta p_b} \qquad (8)$$

where $\cos\theta = 1$ if a liquid which wets the medium is used to fill the pores initially and is displaced by a gas. For this special case the liquid which preferentially wets the solid prevents the interfacial surface between liquid and gas from ever touching the solid; thus one is dealing with a two-phase fluid system, and the porous material is important only insofar as it imposes dimensional limitations on the system. Combined with the value of average pore radius obtained from permeability measurements, the maximum pore radius has proved a useful tool in selection of filter media, the ratio of maximum to average giving some measure of uniformity of pore sizes present. The bubble method can be modified to measure the rate of gas flow at various increasing pressures after the critical pressure for bubbling is reached; by this means a form of pore-size distribution can be calculated as Bechhold (*5*), Grabar (*18*), and Ruemele (*37*) did. The theory and method of calculation involve numerous doubtful assumptions, although these have been clarified recently and the method of calculation has been improved upon by Ishkin and Kazaner (*24*).

PORE-SIZE DISTRIBUTION MEASUREMENT

For packed-bed and woven filter media, two other methods of pore-size measurement are possible which are potentially capable of yielding a complete pore-size distribution curve for almost any type of filter media. The first of these, which is based on physical adsorption of a gas by capillary condensation on the pore walls of the solid, utilizes a modified form of the Kelvin equation. Thus in a circular capillary of radius r, the saturation vapor pressure of a liquid is reduced from p_0 to p_1, where, with a zero angle of contact assumed, p_1/p_0 is given by

$$\ln\frac{p_0}{p_1} = \frac{2\sigma M}{rRT} \qquad (9)$$

For a given liquid at constant temperature, therefore, r is only a function of p_1, provided that σ and ρ_f are constant. It follows that if an adsorption isotherm for a porous medium is drawn as v against p, where v = milliliters of liquid adsorbate per gram of adsorbent, it is necessary only to convert values of p_1 to corresponding values of r to obtain the pore-size-distribution curve. The limitations and difficulties of this method are summarized by Carman (*8*), who has successfully applied it to porous powder plugs with pore radii of 5 to 40 Å., and by Pierce (*33*), who has more recently applied the method successfully over the pore-size range of 25 Å. to 0.1μ. As yet the method has not been successfully applied to the 0.1- to 200-μ pore-radius range, which is of most interest with normal filter media.

The second method capable of yielding a complete pore-size distribution is the liquid-intrusion method first suggested by Washburn (*45*). Because the liquid used must be nonwetting with respect to the porous solid, mercury has been most widely used and the method has become known as the mercury-intrusion method. The method was first successfully applied by Ritter and Drake (*13* and *34*) for the pore-size distribution of such materials as fritted glass, activated clays, diatomaceous earth, and silica gel, covering a pore-radius range from 0.01 to 1.0μ. Drake (*14*) later used the method for further work on the pore structure of catalyst supports. The method was first successfully applied to the textile fabrics by Burleigh and associates (*6*), and this application was more recently extended by Wakeham and Spicer (*44*), and Honold and Skau (*23*). Cotton apparel-type fabrics were examined and an effort was made to correlate interfiber pore volume or radius with air permeability.

The mercury-intrusion method is dependent both on the experimental measurement of the volume of mercury entering the pores of a submerged sample as the absolute pressure is increased and on the relationship between pore size and the pressure required to overcome surface-tension forces and to force mercury into the pores of the sample. When pores of circular cross section are assumed, the pressurizing equation takes the simple form

$$r = (0.1448)\frac{-2\sigma \cos\theta}{p} \qquad (10)$$

where r is radius of pore constriction at which the pressure forces are in equilibrium. When an evacuated sample of a porous material is submerged in a nonwetting fluid such as mercury and subjected to continuously increasing pressure, a unique pressurizing curve of cumulative mercury volume in the sample vs. pressure is obtained if it is assumed that contact angle and surface tension remain constant. On the basis that the volume

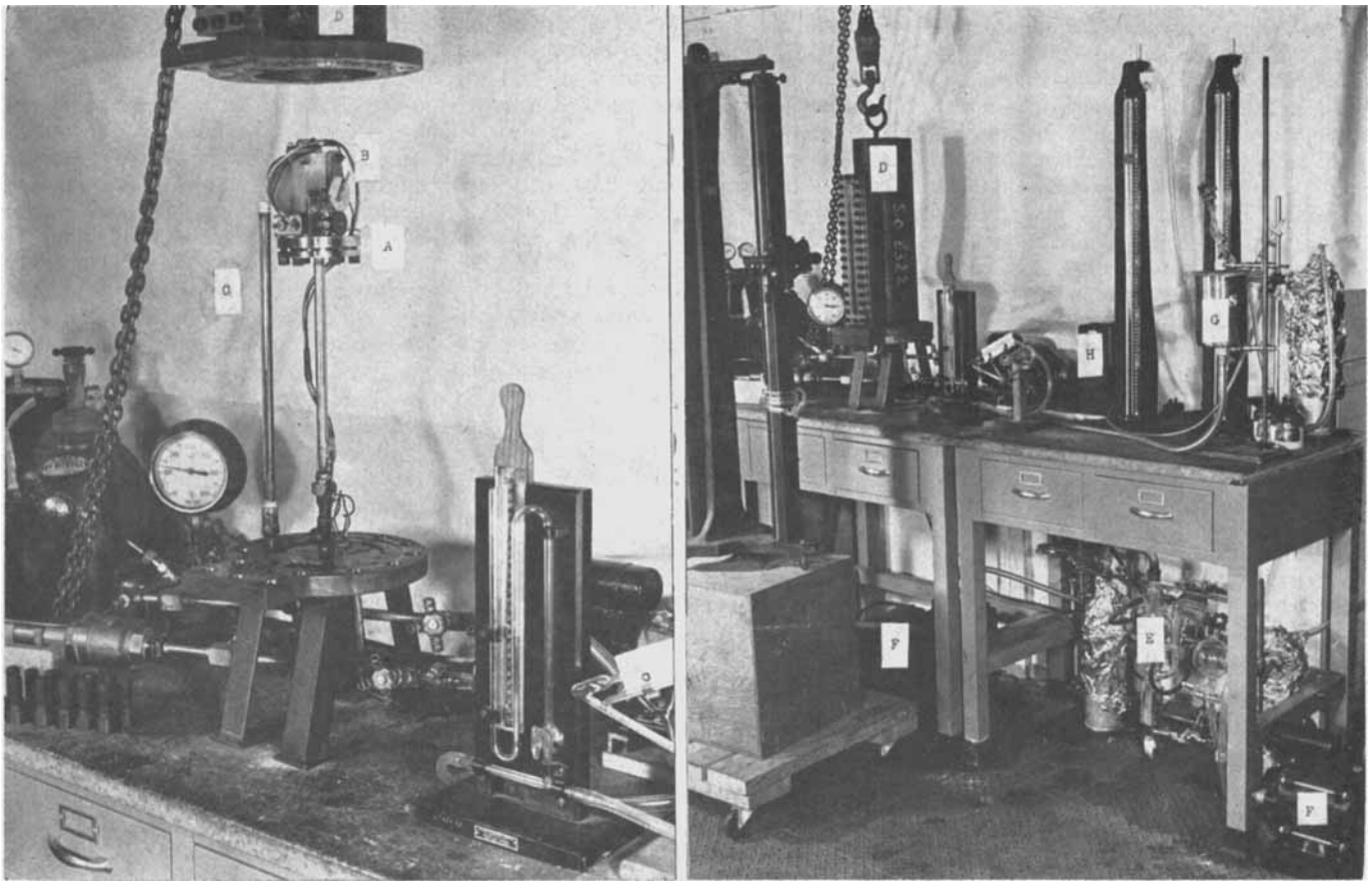

Fig. 1. Dilatometer apparatus for measurement of pore-size distribution: *A*, sample cell; *B*, electric valve; *C*, calibrated capillary, open leg; *D*, dilatometer casing; *E*, diffusion pump; *F*, mechanical forepumps; *G*, mercury reservoir; *H*, squeegee mercury-recirculating pump.

of liquid entering the pores is a function of the radius of the pores as the pressure is increased, a distribution function of pore size can be derived (*34*), and

$$D(r) = \frac{p}{r}\frac{d(\Delta V)}{V_0\, dp} \qquad (11)$$

where r is the radius of pores in equilibrium at absolute pressure p [calculated from Equation (10)] and $d(\Delta V)/V_0\, dp$ is the slope of the pressurizing curve at pressure p, this slope being determined by graphical differentiation.

The assumptions inherent in the application of Equation (11) are that the pore cross section is circular, that σ and θ remain constant during measurements on a single sample, and that satisfactory values of σ and θ are used for each sample. The assumption of circularity of pore cross section is the most likely source of error. If for noncircular pores the "true" pore radius is considered to be the radius of the largest possible inscribed circle, the constant 2 in Equation (10) can be shown to vary between 1.0 and 3.0 for extremes of noncircular pore shape and packing. Therefore, depending on pore shape, the distribution curve obtained from Equation (11), if circular pores are assumed, might be shifted toward either smaller or larger values of pore radius than the "true" pore radius for a noncircular pore. With woven filter media any error may be relatively constant as pore shapes probably do not change radically. Similarly, an error in contact angle or surface tension would have the effect of shifting the derived distribution function on the radius axis. In this work the I.C.T. value of surface tension of mercury in vacuum was used and contact angles between mercury drops and the samples were photographed and measured.

Nonrigidity of the pore system of a material such as a fabric might conceivably lead to compression of the sample during measurement and to distortion of the pore-size-distribution curve. However, with the materials examined, 50 to 90% of the pore volume of the samples were filled at absolute pressures of 10 lb./sq. in. or less, so that sample distortion over this major portion of the distribution curve was minimized. Also, this filling of the major portion of pore volume before the higher pressures were reached stabilized the samples so as to minimize further sample distortion during the remainder of the pressurizing curve. Interpretation of the results in the form

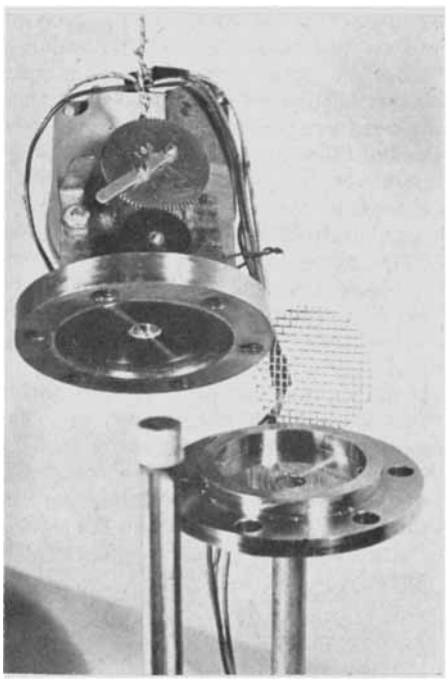

Fig. 2. Dilatometer sample cell with motor-driven valve.

of distribution curves must be tempered by a realization of the probable effect of expansions and contractions in the pore structure. Thus any point on the curves of $D(r)$ vs. r represents pore volume per micron size interval, which can be entered by the mercury only through a constriction of radius r. Thus the effect of such restrictions in either the open pore structure or in closed "ink-bottle" pores results in a hysteresis loop as pressure is released and mercury leaves the pores at the end of the run. This hysteresis effect is similar to that observed for the isotherms in physical-adsorptions measurements, and possible quantitative treatment of this hysteresis effect is discussed by Katz (*25*) and Drake (*14*).

lated through a similarly evacuated reservoir so as to remove air from the solution. After 4-hr. evacuation (absolute pressure usually 10 to 20μ), mercury from the reservoir was introduced into the U tube of the dilatometer until the mercury level rose to the valve level over the sample cell. The valves between the U tube and mercury reservoir were closed, as was the electrically operated valve at the top of the sample cell. Pressurizing of the casing was then started and continued in small increments every 2 to 3 min., a total of 40 to 50 pressurizing steps being included between 0.6 lb./sq. in. gauge and 350 lb./sq. in. abs. Descent of mercury in the open leg of the U tube was observed through the window by means of a cathetometer which allowed the level to be read to the nearest 0.005 cm. The capillary comprising the open leg of the U tube was calibrated against a certified microburette over its entire length of 50 cm., and was found to have a uniform bore capacity of 0.00357 ml./mm. ± 0.00002 ml./mm. over its length. Pressure in the dilatometer casing was raised by bleeding air until atmospheric pressure was reached and by introducing nitrogen at above atmospheric pressure. All pressures up to 15 lb./sq. in. gauge were measured by mercury manometers corrected for barometric pressure. Calibrated Bourdon tube gauges were used from 15 to 350 lb./sq. in. gauge.

Blank runs were made initially in order to correct for any slight expansion of the dilatometer piping during the pressurizing cycle as well as for slight mercury penetration of supporting screens during pressurizing. These blank runs were made with two and four supporting screens present, and

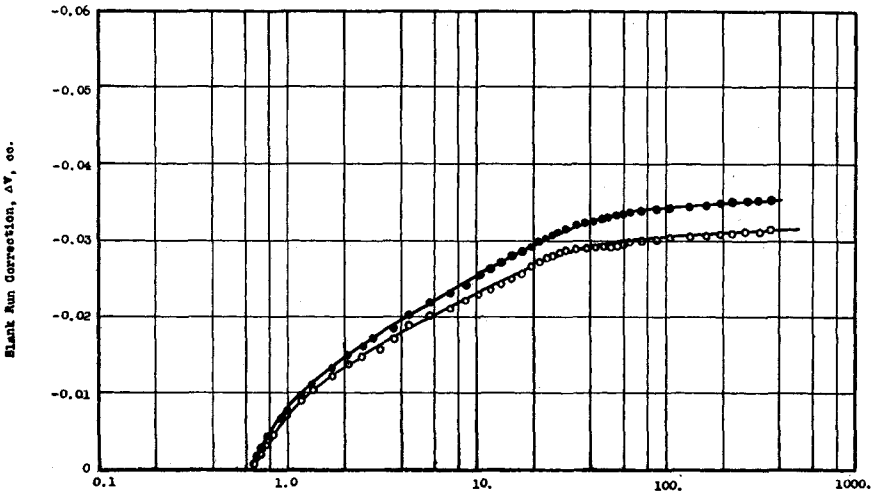

Fig. 3. Dilatometer calibration: blank-run correction curves, no sample; ○ two No. 8-mesh support screens; ● four No. 8-mesh support screens.

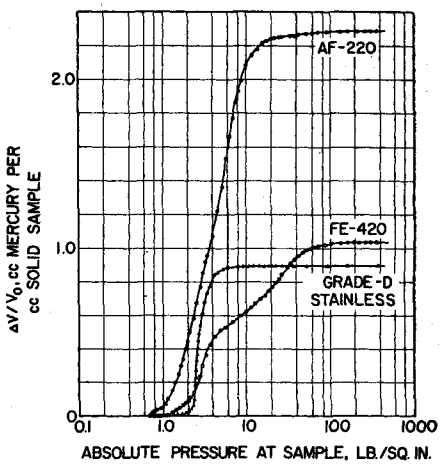

Fig. 4. Dilatometer pressurizing curves; $\Delta V/V_0$, cc. mercury/cc. solid sample.

EQUIPMENT AND EXPERIMENTAL METHODS

For the application of the mercury-intrusion method to most woven and packed-bed filter media, a pore-radius range of 0.3 to 180μ must be covered. This corresponds roughly to an absolute pressure range of 0.6 to 350 lb./sq. in. Such a range had not previously been covered by a single dilatometer, the only reported work over this range (*23*) requiring three separate dilatometers. In order to make uninterrupted pore-size measurements over this entire range by use of a single sample of filter medium, the U-tube dilatometer shown in Figures 1 and 2 was designed and constructed. This U-tube dilatometer (Figure 1*a*) has the sample cell and an electrically driven valve at the top of one leg and the other leg consists of the calibrated capillary with open end. The sample was held in a horizontal plane between 8-mesh stainless steel screens within the sample cell, which is shown disassembled in Figure 2. Before the mercury is introduced, the entire dilatometer casing (shown closed and assembled with accessory equipment in Figure 1*b*) was evacuated by a mechanical forepump and mercury-diffusion pump. Meanwhile the system mercury was circu-

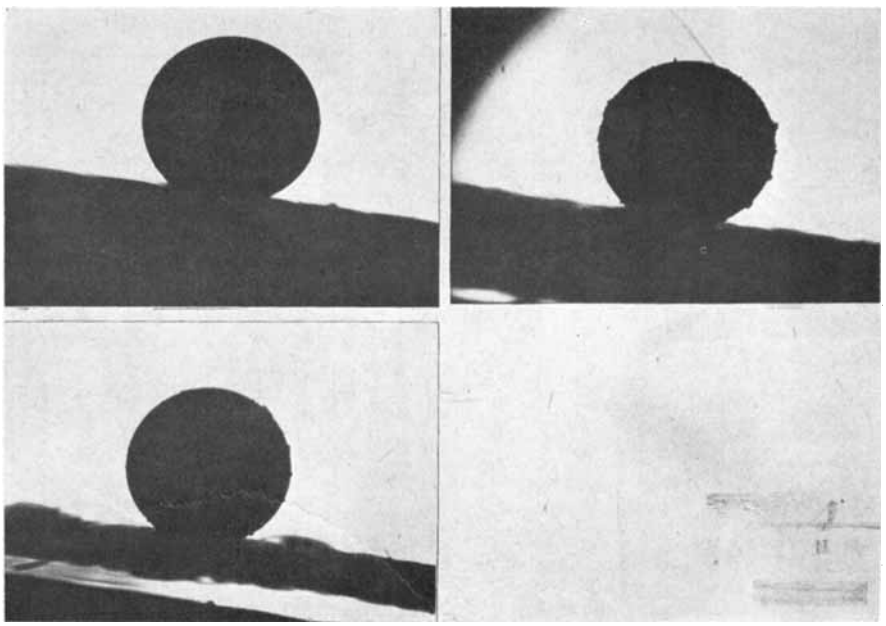

Fig. 5. Photomicrographs of contact angle between mercury and filter medium (filter medium inclined 10° from horizontal): top left, TF-5071-F Orlon, θ_A = 147°; top right, FE-420 Orlon, θ_A = 150°; bottom left, TF-5044 nylon, θ_A = 145°.

TABLE 1. DATA ON FILTER-MEDIA SAMPLES SUBJECTED TO MERCURY-INTRUSION MEASUREMENTS AND CLARIFICATION EVALUATIONS

Filter medium style or type	Yarn construction	Weave	Thread count/in. warp × fill	Wt., oz./sq. yd.	Thickness, in.	Porosity ϵ, void fraction	% Pore volume filled during measured portion of dilatometer run	Mercury-sample contact angle used	Modal pore sizes by mercury intrusion, μ: Inter-fiber pore radius	Modal pore sizes by mercury intrusion, μ: Inter-yarn pore radius	Permeability determined: Avg. pore radius*, μ	Permeability determined: Radius of maximum pore†, μ	Permeability determined: Liquid-resistance coefficient R_m, 1/ft. × 10^6	Permeability determined: Air-resistance coefficient R''_m,	Permeability determined: Air Permeability** (cu. ft.)(min.)/sq. ft.
Turner-Halsey 8 cotton duck	Spun staple	Plain	45 × 28	17.9	0.0350	0.537	95.9	140	2.9	55	0.90 (3.8)‡	12.4 (22.6)‡	13,600 (710)‡	413	1.0
National 33 (175-TW) cotton	Spun staple	Twill	37 × 25	17.9	0.0440	0.603	97.9	140	5.3	54	4.1 (9.9)‡	44 (44)‡	680 (116)‡	47	8.8
Wellington-Sears SN-23 nylon	Spun staple	Plain	50 × 29	14.9	0.0352	0.505	91.4	145	4.0	40	5.2	91	388	118	3.5
Feon 420 Orlon	Multifilament (moderate twist)	Satin	200 × 128	5.94	0.0140	0.517	96.4	150	3.9	42	8.0	83	72	34	12.3
Stehli 5044 nylon	Multifilament	Twill	220 × 125	3.55	0.0070	0.413	99.4	145	3.0	116	5.5	29	88	109	3.8
Stehli 5071-U Orlon (Edco HT-16-UF)	Multifilament, high-twist yarns	Taffeta	76 × 24	13.1	0.0320	0.528	69.8	150	3.8	29	14	71	44	26	16
Stehli 5071-F Orlon (Edco HT-16-F)	Multifilament, calendered, high-twist yarns	Taffeta	80 × 21	13.0	0.0210	0.296	92.8	150	2.2	25	5.4	39	380	243	1.7
Wellington-Sears SN-7 nylon	Multifilament (low twist)	Plain	60 × 42	6.32	0.0155	0.523	39.0	145	5.0	> 180	10.5	128	44	31	13.5
Albany 220 wool felt	Staple	Woven base felt	..	35.8	0.120	0.701	97.4	140	16.5	..	3.2 (15.0)‡	21 (24)‡	.. (118)‡	67	6.2
Micrometallic grade *D*, porous stainless steel	Pressed and sintered metallic powder	..	..	38.4	0.129	0.485	94.1	140	43.0	..	36.5	63			

*Calculated from water-permeability measurements by method of Equations (4) to (6).
†Calculated from maximum bubble-pressure measurements with air-water, by method of Equation (8).
‡Calculated as above, but from measurements with carbon tetrachloride instead of water.
**At Δp = 0.5 in. water and 70°F.

the correction curves of Figure 3 were obtained for subsequent use in correcting pressurizing curves obtained with various media. Size of samples of filter medium used in each run were chosen so as to yield a final mercury depression in the capillary of at least 25 cm., and size varied from 0.5 to 9 sq. in. depending on medium thickness. With very thin media, two or three layers of sample were used with screens between layers. The inside of the sample cell was 5.8 cm. diam. by 0.5 cm. in height, the samples being held at the desired vertical level by the screens.

In Figure 4 are shown typical pressurizing curves. For convenience, these curves were normally plotted on arithmetic paper and successive tangents taken. Thus values of $d(\Delta V)/V_0\,dp$, the slopes of the pressurizing curve, were obtained for various values of p, permitting calculation of the distribution function $D(r)$ from Equation (11). The values of contact angle θ, needed for application of Equations (10) and (11), were obtained directly from photographs of a mercury droplet resting on an inclined sample of each filter medium. The mercury droplet was 1.8 to 2.0 mm. in diameter in each case and was photographed resting on a clean piece of filter medium inclined at a 10° angle. The advancing contact angle was measured directly on these photographs, several of which are shown in Figure 5. The values obtained ranged from 136 to 152°. Values of 140° for cotton, wool, and stainless steel, 145° for nylon, and 150° for Orlon acrylic fiber were used in the calculations. The surface tension of mercury was taken as the I.C.T. value in a vacuum, the value at 25°C. being 475 dynes/cm.

The porosity or void fraction of all samples was determined independently with the gravimetric method, by use of the established density for the base fiber material. The air and liquid permeabilities of 2-in.-diam. samples were determined over a range of pressure drops representative of viscous-flow conditions, and the respective resistance coefficients were calculated by means of Equation (6). The effective specific surface of the medium and its average pore radius were calculated from this liquid resistance coefficient and the measured porosity, Equations (4) and (5) being employed. Liquid-saturated samples of 2-in. diam. were also subjected to the bubble-pressure test, and the results of five measurements of bubble pressure were averaged for use with Equation (8) in the calculation of maximum pore size.

DISCUSSION OF RESULTS

The ten types of filter media examined are listed in Table 1 together with various data on their physical properties, liquid resistance, air permeability, average pore size, and size of maximum pore. Table 1 also shows that with these samples 90 to 100% of the independently measured pore volume was filled with most media during the measured portion of the dilatometer run, although excessive surface roughness decreased this figure with two of the media. The pressurizing curves, as typified by those of Figure 4, show that in all cases the filling of the pores had practically ceased by the time 350 lb./sq.

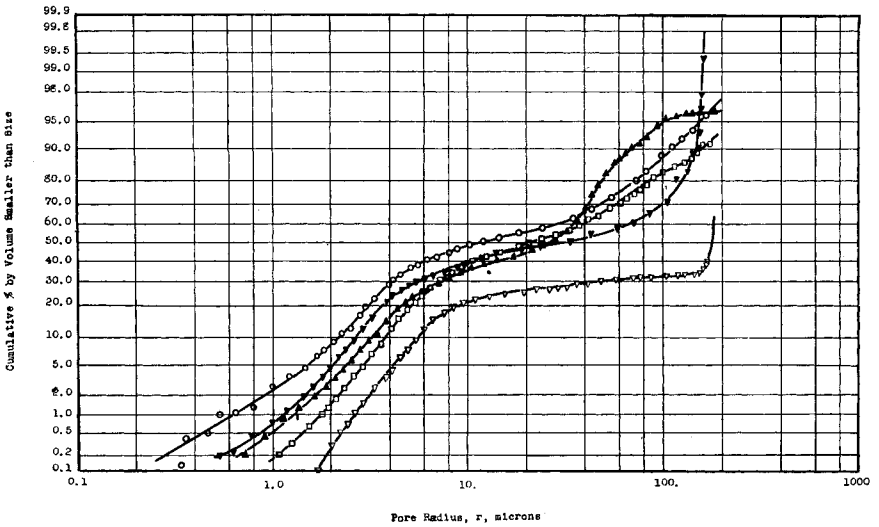

Fig. 6, Cumulative pore-size distribution curves: ○ No. 8 staple cotton duck; □ SN-23 staple nylon duck; ▲ FE-420 filament Orlon satin; ▽ SN-7 filament nylon duck; ▼ TF-5044 filament nylon twill.

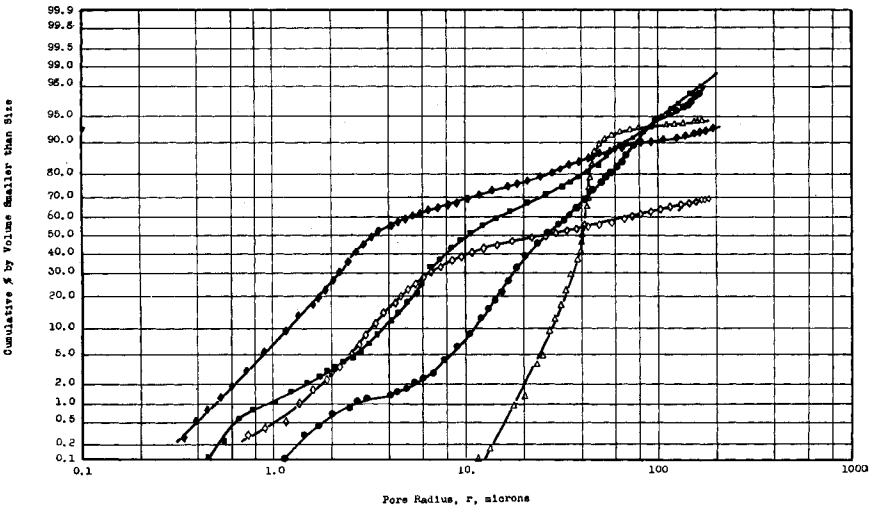

Fig. 7. Cumulative pore-size distribution curves: ● Albany No. 220 wool felt, ◇ Stehli TF-5071-U Orlon taffeta; ◆ Stehli TF-5071-F finished Orlon taffeta; △ Grade D porous stainless steel; ■ TW-175 staple cotton twill.

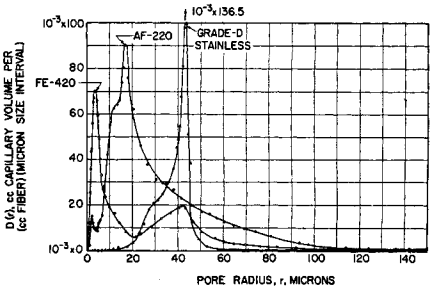

Fig. 8. Pore-size distribution: $D(r)$, cc. capillary volume/(cc. fiber) (micron size interval).

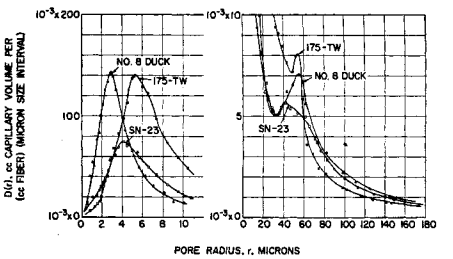

Fig. 9. Pore size distribution: $D(r)$, cc. capillary volume/(cc. fiber) (micron size interval).

in. abs. pressure was reached, an indication of the existence of negligible pore volume not yet filled at this final pressure. Thus the major portion of the unfilled pore volume probably represents large surface pores of the medium which are filled by mercury at less than 0.6 lb./sq. in. abs. pressure. These large surface pores characterize the surface roughness of the medium.

Figures 6 and 7 show cumulative pore-radius-distribution curves, plotted according to particle size, for the ten media. These curves are based on the premise that essentially all pore volume is filled at 350 lb./sq. in. abs. pressure; thus pore volume not filled during the measured portion of the dilatometer run is assumed to be filled below 0.6 lb./sq. in. abs., which was the starting pressure. Curves of the pore-size-distribution function $D(r)$ are presented in Figures 8, 9, and 10. These curves were calculated directly from Equations (10) and (11), no assumptions concerning unfilled pore volume being involved.

Woven-fabric Media

In the woven-fabric media the measured pore volume was distributed between interyarn or interthread pores and interfiber pores within the yarn structure. The cumulative size-distribution curves of Figures 6 and 7 show that with all woven media 30 to 50% of the pore volume was measured at a radius of less than 10μ and probably represents mainly that portion of the pore volume existing as interfiber voids. This is confirmed by the curves of $D(r)$ vs. r of

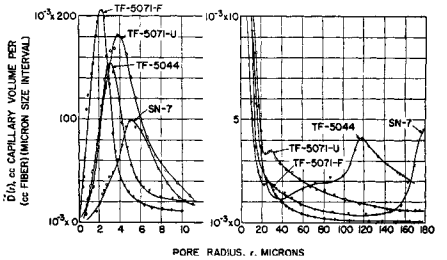

Fig. 10. Pore-size distribution: $D(r)$, cc. capillary volume/(cc. fiber) (micron size interval).

Figures 8 to 10, which for these same woven media show a sharp maximum at pore radius less than 10μ in each case, and a second less well defined maximum in the pore-radius range of 25 to 125μ. The sharp maximum below 10-μ radius appears to represent the "modal" interfiber pore radius; whereas the less distinct maximum above 25μ may represent the modal interyarn-pore radius. Actually the region over which the interyarn pores are filled is quite broad, extending from the radius of maximum pore, as measured by the bubble-pressure method, to a size approaching that of the largest interfiber pore. The sharpness of this secondary maximum appears to be much greater with a satin weave (FE-420 medium of Orlon acrylic fiber) than with the plain or taffeta weave. This may result from the fact that a satin weave embodies a greater tortuosity of interyarn pores than does a plain or taffeta weave. In some cases (Table 1) the modal value of the interyarn-pore radius was greater than the radius of maximum pore measured by the bubble-pressure method; the reason for this is not clear but probably involves complications of interyarn-pore shape which invalidate direct comparison of results.

In general the average pore radius calculated from independent permeability measurements (Table 1) falls between the modal value of interfiber pore radius and the modal value of interyarn pore radius. This would be expected if flow through the medium occurs by passage in parallel through both interyarn and interfiber pores. This is true even with the staple cotton media provided the average pore radius is calculated from permeability measurements with a liquid which does not swell the cotton fibers.

Although the Stehli 5071-U (Edco HT-16UF) and 5071-F (Edco HT-16-F) styles are constructed with unusually high-twist yarns (approximately 15 turns/in. on 600-denier yarn containing 400 filaments of 1.5 denier), Figure 7 shows that 40% of pore volume of the former style and 70% of pore volume of the latter measures smaller than 10μ and probably occurs as interfiber pores. This finding is in contrast to the views of Smith (*42*), who has stated that the yarns of such high-twist media are essentially impervious to flow and approach a monofilament in filtering action. Smith based his views on semiquantitative observation of comparative flow through media woven from ordinary yarns and from yarns which were intentionally loaded before weaving in an effort to saturate interfiber pores. It is likely that the yarn-loading process used by Smith may have been ineffective with the higher twist yarns, leading to the false conclusion that the absence of a decrease in permeability on loading meant that the original yarns were necessarily impervious. The effect on pore-size distribution of finishing by calendering and heat-treatment is shown by comparing the curves of Figures 7 and 10 for 5071-U and 5071-F, the latter being the same as the former except for finishing. Figure 7 shows little change in the shape of the size-distribution curve, but rather a shift of the entire curve. Figure 10 shows that much of the pore volume originally present as surface roughness and interyarn pores has been eliminated and that size of both interyarn and interfiber pores has been reduced. This is in general agreement with the findings by independent measurements of average and maximum pore radius in Table 1. In general these findings on high-twist media, in both the unfinished and finished conditions, indicate that the effectiveness of high-twist yarns in improving the performance of filter media does not result from elimination of flow through yarn structure by the forming of impervious yarns as reported by Smith (*42*). Rather it appears that the effectiveness of high-twist yarns depends only on reduction in size of the interfiber pores.

Thus, the size of interfiber pores is reduced below the size allowing particle penetration and plugging with a particular system, but yarns remain permeable and a large part of filtration continues to occur through the interfiber pores. In contrast, the effect of finishing appears to result from reduction in size of both interfiber and interyarn pores, with the predominant effect that of eliminating a large part of the interyarn pore volume. In fact these data indicate that when both high twist and finishing are combined, an abnormally high percentage of pore volume exists as interfiber voids and an even greater proportion of filtration action may occur through the yarn structure than occurs with low-twist media which are unfinished. This finding suggests that progressive plugging of a filter medium in cake-filtration service can be prevented only when a medium is selected with an interfiber pore radius sufficiently small to prevent penetration of the yarn structure by the smallest particles or particle agglomerates existing in the feed suspension. The value of a combination of high-twist yarns and the finishing method, which is employed by Stehli & Co. and by Edco as a means of reducing filter media plugging, therefore appears to accrue from (1) a reduction in interfiber pore size caused both by high-twist yarns and by finishing, and (2) a marked reduction in interyarn pore volume and size caused by the finishing operation alone.

Felt Media

Because of the more random orientation of fibers in felt media, a much higher porosity results and a much broader range of pore-size distribution might be expected. The single felt examined (Albany 220 of Table 1) is a woven-base felt. Such felts are made by weaving a loose base structure which is roughed and worked to form a felt surface on both sides of the base structure. The medium exhibited a much larger average pore size than the woven media, 90% of the pore volume being measured as above 10-μ radius (Figure 7). With this material the large peak at 10 to 20μ on the $D(r)$ curve of Figure 8 represents the modal size of interfiber pores in the bulk of the felted structure and the very slight inflection at 2- to 3-μ radius is indicative of modal size of interfiber pores in the woven-base structure. Average pore size calculated from permeability data agreed closely with the modal size of the interfiber pores in the bulk of the felted structure (Table 1) when a liquid was used which did not swell the fibers. The $D(r)$ curve of Figure 8 indicates that for felt media the interfiber pores in the bulk of the felt structure cover a greater range of size within a given medium than do interfiber pores of a woven-fabric type of medium.

Sintered-metal Media

Under this class a sample of grade *D* porous stainless steel (Table 1) was examined. Results showed the pore-size distribution of this type of medium to be much narrower than that of either woven fabrics or felt. Thus with the sample examined, 90% of the pore volume was measured as falling between 20 and 50μ of pore radius (Figure 7). The sharpness of the frequency distribution as compared with a fabric and a felt are shown by the $D(r)$ curves of Figure 8. The average pore radius of 36.5μ (Table 1) calculated from water-permeability data by means of Equations (4) and (6) appears in excellent agreement with the experimentally determined size distribution. This indicates that the porous stainless steel medium approximates a random-packed bed and that the assumptions of the Kozeny-Carman equation must be reasonably valid as applied to this particular material.

SUMMARY

It has been shown that the mercury-intrusion method can be successfully applied to determine the pore-size distribution of filter media. Following are the results of such measurements on typical filter media.

1. Pore-size distributions so obtained are compatible with pore-size information obtained by the permeability and bubble-pressure methods, but the pore-size distributions resulting from mercury-intrusion measurements are much more informative in regard to pore structure.

2. With woven filter media the pore volume is distributed between interyarn and interfiber pores, with 30 to 50% of the pore volume existing as interfiber pores even with media constructed of high-twist yarns.

3. The finishing of woven filter media by calendering and heat setting reduces the size of both interyarn and interfiber pores

while reducing the proportion of pore volume existing as interyarn pores.

4. With felt media the pore volume exists as interfiber pores which are distributed in size over a much wider range than are the interfiber pores of woven media.

5. With consolidated porous media the size distribution of pore volume is very narrow compared with that with woven or felt media.

Further application of the mercury-intrusion method to the study of the internal structure of filter media can be expected to define, with textile media, the effect of yarn packing, filament and yarn denier, staple length, yarn crimp and ply, and various finishing treatments. Similar application to consolidated porous media can be expected to define the effect of particle-size distribution, particle shape, consolidating pressure, and sintering conditions. However, the accumulation of such information on both types of filter media will lead to a more systematic design of filter media only if filtration studies can successfully correlate pore structure with particle size removed and rate of plugging of the medium.

NOTATION

A = superficial filtration area at surface of filter medium or cake deposited thereon, sq. cm.

b = empirical constant in Reinard's equation, dimensionless

C_1 = inertial coefficient in empirical equation, g.sec.^{2}/cm.^{3}

C_2 = viscous coefficient in empirical equation, g.sec./cm.^{5}

$D(r)$ = frequency-distribution function of pore volume in terms of pore size through which it is accessible to a penetrating fluid, (cc. pore volume)/(cc. solid)(μ size interval)

g_c = conversion factor in Newton's law of motion, 980 (g.)(cm.)/(g.force)(sec.)^2

h = effective pore length, cm.

K = constant of Kozeny-Carman relationship (5 $\pm$ 10%), dimensionless

L = thickness of filter medium, ft.

m = average hydraulic pore radius, cm. [$= r_p/2$ for circular pore; $= \epsilon/(1-\epsilon)S_0$ for packed bed]

M = molecular weight of liquid adsorbate used in capillary adsorption measurements, g./mole.

N = number of pores per unit area, 1/sq. cm.

p = absolute pressure at filter medium, lb./sq. in.

p_0 = saturation vapor pressure in bulk of a liquid absorbate, mm. Hg

p_1 = saturation vapor pressure of a liquid in capillary of radius r, mm. Hg

Δp_b = pressure drop across unused medium when first bubble of gas is passed in bubble-pressure method, lb./sq. in.

Δp_f = pressure drop across unused medium with single fluid phase flowing, lb./sq. in.

Δp_w = pressure drop across unused medium in liquid-permeability measurements, lb./sq. in.

q_f = rate of fluid passage through unused filter medium, cc./sec.

r = pore radius in medium, μ

r_p = average pore radius of filter medium calculated from liquid-permeability measurements, μ

r_m = radius of maximum size of pore calculated from bubble-pressure measurements, μ

r_f = modal value of interfiber pore radius as measured by mercury-intrusion method, μ

R = gas constant, calories/g. mole

R_m' = resistance of unused filter medium determined by liquid-permeability measurements in viscous range, 1/ft.

R_m'' = resistance of unused filter medium determined by air-permeability measurements, 1/ft.

S_0 = specific surface of filter medium, sq. cm./cc. fiber

T = absolute temperature, °Kelvin

v = volume of liquid adsorbate/unit solid absorbent, cc./g.

V_0 = volume of fiber solids in test specimen (mercury-intrusion method), cc.

$\frac{\Delta V/V_0}{V_0\, d_p}$ = cumulative volume of mercury having entered pores of filter medium under test (mercury-intrusion method) at absolute pressure p, cc./cc. fiber

$d(\Delta V)$ = slope of pressurizing curve at pressure p (mercury-intrusion method), (cc. pore volume)/(cc. fiber)(lb./sq. in.)

ϵ = porosity of filter medium, void fraction, dimensionless

ρ = density of liquid absorbate, g./cc.

ρ_f = density of flowing fluid, g./cc.

σ = surface tension, dynes./cm.

μ_f = viscosity of solution or filtrate, centipoises

θ = advancing contact angle, degrees

LITERATURE CITED

1. Anon., "Handbook of Technical Data on Wire Cloth and Filter Cloth," Catalog 50, Multi-Metal Wire Cloth Co., Inc., New York (1950).
2. Anon., "Physical Separation of Immiscible Fluids Through Porous Media by Means of Surface and Interfacial Tension," Selas Co., Philadelphia (1943).
3. Backer, S., *Textile Research J.*, **21**, 703 (1951).
4. Bechhold, H., *Z. physik. Chem.*, **64**, 328 (1908).
5. ———, *Kolloid-Z.*, **66**, 334 (1934).
6. Burleigh, E. G., Jr., H. Wakeham, E. Honold, and E. L. Skau, *Textile Research J.*, **19**, 547 (1949).
7. Carman, P. C., *Ind. Eng. Chem.*, **31**, 1047 (1939).
8. ———, *Proc. Roy. Soc. (London)*, **209A**, 69 (1951).
9. Cummins, A. B., *Ind. Eng. Chem.*, **34**, 403 (1942).
10. Cunningham, G. E., G. Broughton, and R. R. Kraybill, *Ind. Eng. Chem.*, **46**, 1196 (1954).
11. Davies, C. N., *Arhiv. Hi. Rada*, **1**, 4 (1950); *Proc. Inst. Mech. Engrs. (London)*, **1B**, 185 (1952).
12. Deadmore, D. L., *Ceram. Age*, **56**, 15, 23 (1951).
13. Drake, L. C., and H. L. Ritter, *Ind. Eng. Chem.*, **37**, 787 (1945).
14. Drake, L. C., *Ind. Eng. Chem.*, **41**, 780 (1949).
15. Durwez, P., and L. Green, *J. Appl. Mechanics*, **18**, 39 (1951).
16. Elford, W. J., *Proc. Roy. Soc. (London)*, **B112**, 384 (1933).
17. Ergun, S., *Chem. Eng. Progr.*, **48**, 89 (1952).
18. Grabar, P., and J. Nikitine, *J. chim. phys.*, **33**, 721 (1936).
19. Grace, H. P., *Chem. Eng. Progr.*, **49**, 303 (1953).
20. Hoerner, S. F., *Textile Research J.*, **22**, 274 (1952).
21. Hoffing, E. H., and F. J. Lockhardt, *Chem. Eng. Progr.*, **47**, 3 (1951).
22. Hoffman, R. M., *Textile Research J.*, **22**, 170 (1952).
23. Honold, E., and E. L. Skau, *Textile Research J.*, **21**, 419 (1951).
24. Ishkin, I. P., and M. G. Kazaner, *Zhur. Fiz. Khim.*, **24**, 943 (1950).
25. Katz, S. M., *J. Phys. & Colloid Chem.*, **53**, 1166 (1945).
26. Knoll, H., *Kolloid Zhur.*, **90**, 189 (1940).
27. Langmuir, I., "Smokes and Filters," No. 865, Part IV, U. S. Office Sci. Res. & Dev. (1942).
28. Madras, S., *Can. J. Research*, **27B**, 764 (1949).
29. Manegold, E., *Trans. Faraday Soc.*, **33**, 1088 (1937).
30. McBain, J. W., and S. S. Kistler, *loc. cit.*, **26**, 157 (1930).
31. Morton, T. H., *loc. cit.*, **31**, 267 (1935).
32. Penner, S. E., and A. F. Robertson, *Textile Research J.*, **21**, 775 (1951).
33. Pierce, C., *J. Phys. Chem.*, **57**, 149 (1953).
34. Ritter, H. L., and L. C. Drake, *Ind. Eng. Chem.*, **17**, 782 (1945).
35. Rainard, L. W., *Textile Res. J.*, **17**, 167 (1947).
36. Robertson, A. F., *loc. cit.*, **20**, 838, 844 (1950).
37. Ruemele, T., *Z. Anal. Chem.*, **119**, 360 (1940).
38. Schwarz, E. R., *Textile Research J.*, **21**, 125 (1951).
39. Schwertz, F. A., *J. Appl. Phys.*, **20**, 1070 (1949).
40. Segall, G. H., *Textile Res. J.*, **22**, 736 (1952).
41. Silverman, L., *Heating and Ventilating*, **47**, 68 (1950).
42. Smith, E. G., *Chem. Eng. Progr*, **47**, 545 (1951).
43. Thomas, D. J., *J. Inst. Heating, Ventilating Engrs. (London)*, **20**, 35 (1952).
44. Wakeham, H., and N. Spicer, *Textile Research J.*, **19**, 703 (1949).
45. Washburn, E. W., *Proc. Natl. Acad. Sci. U. S.*, **7**, 115 (1921).